International Journal of Heat and Mass Transfer 87 (2015) 49–58

Contents lists available at ScienceDirect

International Journal of Heat and Mass Transfer

journal homepage: www.elsevier.com/locate/ijhmt

Experimental and numerical investigation of 3D gas flow temperature field in infrared heating reflow oven with circulating fan

A.M. Najib [a,b], M.Z. Abdullah [a], C.Y. Khor [a,*], A.A. Saad [a]

[a] Advance Packaging and SMT Unit, School of Mechanical Engineering, Universiti Sains Malaysia, Engineering Campus, 14300 Nibong Tebal, Penang, Malaysia
[b] Advance Mechatronic Laboratory, Faculty of Manufacturing Engineering, Universiti Teknikal Malaysia Melaka, Hang Tuah Jaya, 76100 Durian Tunggal, Melaka, Malaysia

ARTICLE INFO

Article history:
Received 8 September 2014
Received in revised form 22 March 2015
Accepted 23 March 2015

Keywords:
Desktop lead-free reflow oven
CFD
Forced-air convection
IR heating

ABSTRACT

This study presents the experimental and numerical analysis of the thermal process for laboratory scale desktop lead-free reflow oven and discusses a 3D CFD model of radiation heating with forced-air convection from circulating stainless steel fan. The experiments were carried out to determine the temperature boundary condition of infrared heating element. In addition, the RPM of the rotating fan was measured using HT50 tachometers. To validate the spatial temperature of the oven, a set of industrial standard thermocouples was employed in various positions. The device was accessed throughout all stages of temperature reflow profile. The profile setting of the oven is in accordance to standard JSTD-020D. The desktop reflow oven was then numerically simulated using the computational model and the advanced user-defined functions (UDFs) were developed to model the thermal profile. The study reveals the temperature distribution of the desktop reflow oven is dependent on the air circulation in the oven at various positions. The temperature contour and air circulation in the oven chamber were demonstrated in the numerical simulation. The experimental and simulation results are useful for further improvement of temperature uniformity within the oven chamber for a convective IR heating reflow oven. The temperature results show a satisfactory agreement with both experiment and simulation.

1. Introduction

Reflow oven is widely used in the microelectronics industry to assemble surface mount components (SMCs) and devices (SMDs) onto the printed circuit board (PCB). Prior to the reflow soldering process, the solder paste is printed on the copper pad which covered by surface finishes (e.g. ENIG, Imm Ag, Imm Sn, etc.). Then, the automated placement machine deposits the SMCs on the solder paste. After that, the PCB passes through different zones (i.e., preheating, soaking, soldering and cooling) in the reflow oven. Typically, two types of the reflow oven have been used based on the scale and the application. Multiple zones reflow oven is commonly used in the industry for the mass production of the assembly process. On the contrary, the desktop reflow oven is appropriate for low-volume production and research purpose. In general, the PCB inside the desktop reflow oven is static at its location, whereas the PCB inside the reflow oven with multiple zones is carried by conveyor throughout different stages. The most commonly used reflow ovens today were forced convection, infrared (IR) and the combination of two [1]. The IR reflow oven can be classified by heating principle of the device. Reflow oven with medium and long wave required additional air convection for temperature field distribution within the oven space. The airflow can circulate either a forced or natural manner. Forced air circulation is usually implemented using a fan or jet impingement system. The air circulation introduced in an infrared oven is to ensure uniform temperature distribution within the space.

The characteristics of the reflow oven depend on the oven design (e.g., multiple sections or single chamber), the heating device and airflow control (e.g., fan or jet impingement system). The understandings of the reflow oven are significant to the process control in the reflow soldering process. Reflow soldering profile may influence the microstructure of the solder joint, such as thickness of intermetallic compound (IMC) [2]. High peak reflow temperature and longer time above the liquidus temperature contribute to the increase of the IMC layer. The solder joint with a thick layer of IMC is prone to failure during the thermal cycle [3]. Besides, it degrades the mechanical properties and leads to brittle failure mode [4,5]. The homogeneity and efficiency of the reflow oven have the crucial impact on the solder joint reliability. The inhomogeneous temperature distribution in the reflow oven may

* Corresponding author. Tel.: +60 195637283; fax: +60 4 594 1025.
E-mail addresses: cykhor_1985@hotmail.com, mecykhor@usm.my (C.Y. Khor).

http://dx.doi.org/10.1016/j.ijheatmasstransfer.2015.03.075
0017-9310/

Nomenclature

$C_{1\varepsilon}$, $C_{2\varepsilon}$, $C_{3\varepsilon}$	model constant –
C_P	specific heat J/kg-K
D	fan diameter m
F_i	force in the ith-direction N
G_k	turbulence energy J
g_i	gravitational acceleration N/m^2
$I(r, s)$	directionally and spatially dependent radiation intensity W/m^2-sr
n	rotational speed rpm
p	pressure Pa
T	temperature K
t	time s
u_i	fluid velocity component (i = 1, x-direction; i = 2, y-direction; i = 3, z-direction) m/s
x_i	Cartesian coordinates (i = 1, x-coordinate; i = 2, y-coordinate; i = 3, z-coordinate) m

Greek letters

α	absorption coefficient J//kg
α_s	swirl factor –
λ	thermal conductivity W/m-K
μ	viscosity Pa s
ρ	density kg/m^3
σ	Stefan–Boltzmann constant W/m^2 K^4
σ_s	scattering coefficient sigma 1/m
τ_{ij}	viscous stress tensor N/m^2

lead to the reflow soldering failures [6]. Therefore, the reflow oven studies on various aspects had been reported by the scholars. The experimental and simulation investigations of the reflow oven include heat transfer coefficient [7], construction of a convection reflow oven [8] and gas flow characterization [9]. The nozzle-matrix convection reflow oven [5–9] was extensively used in the previous studies. Besides, the contamination of the nozzles [6,10] causes inhomogeneous temperature and affects the heating efficiency. Routine maintenance and service to clean the nozzles are significant to maintain the oven efficiency in the electronics assembly industry.

Besides, vapor phase soldering (VPS) has been used as a new and spreading alternative of the small series surface mount technology (SMT). The modeling of vapor phase soldering had been investigated by a few scholars in recent years [11–14]. Multi-physics modeling approach [11] was applied to model the combined transport mechanism during the VPS process. Temperature and vapor concentration were reported as the main parameters in the vapor phase soldering. Illés and Géczy [12] extended the investigation of the dynamic changes of the vapor concentration in VPS oven. Board level modeling was considered for the vapor concentration. Géczy et al. [13] studied filmwise condensation heat transfer based on Nusselt theory. Both sides (i.e., top and bottom) of the PCB were combined to obtain an overall heat transfer coefficient during the VPS process. They found the application of filmwise condensation model is more practical compared with complex multi-physic model. Furthermore, application of dynamic condensate layer [14] improved the accuracy of the numerical modeling in the VPS process.

The understandings of desktop reflow oven facilitate the researcher to control the reflow profile during the soldering process. Lau et al. [15] employed a desktop reflow oven in the optimization of the ball grid array (BGA) packaging using Taguchi method. The oven heating element is using infrared and fan convection. The reflow profile setting controls the temperature in the oven chamber. The BGA is static during the reflow soldering process; inhomogeneous temperature distribution may easily lead to over or insufficient heating to the PCB and components. This research field remained a gap in the study of thermal characteristics of reflow oven. In addition, in-depth study of the desktop reflow oven still not available in the literature. Therefore, this study aims to fill the research gap by using the desktop reflow oven. The oven thermal characteristics during the reflow soldering process were investigated in the experiments and simulations. Temperature distribution in the oven chamber at various positions, heights and fan speed were studied. The experimental measurement values were then validated by the simulation results.

2. Governing equations

The airflow in the oven is assumed incompressible, and the governing equations describing the fluid flow are conservation equations of mass and momentum. FLUENT normally solves the governing equations using Cartesian spatial coordinates and velocity components.

Eq. (1) is the simplified form of the mass conservation equation and is valid for incompressible flows.

$$\frac{\partial \rho u_i}{\partial x_i} = 0 \tag{1}$$

Conservation of momentum in ith direction in an inertial (non-accelerating) reference frame is described by:

$$\frac{\partial}{\partial t}(\rho u_i) + \frac{\partial}{\partial x_j}(\rho u_i u_j) = -\frac{\partial P}{\partial x_i} + \frac{\partial \tau_{ij}}{\partial x_j} + \rho g_i + F_i \tag{2}$$

where, P is the static pressure, τ_{ij} is the viscous stress tensor, g_i, is the gravitational acceleration and F_i is external body force in the ith-direction.

The energy equation is also solved and can be written as,

$$\frac{\partial}{\partial t}(\rho C_p T) + \frac{\partial}{\partial x_i}(\rho u_i C_p T) = \frac{\partial}{\partial x_j}\left(\lambda \frac{\partial T}{\partial x_i}\right) + S_h \tag{3}$$

where C_p, T and λ are the specific heat capacity, temperature and thermal conductivity of the air, respectively. Energy source due to radiation are included in the energy source term S_h.

The radiative heat transfer occurs in the oven chamber. The desktop oven filled with heated atmospheric air was computationally complex when using this type of geometry and the thermal radiation requires application of specific radiation model. As reported by Smolka et al. [16], the discrete ordinates (DO) model was selected from a number of radiation models that available in the ANSYS Fluent software.

To account for radiation, radiative transport equation using DO model [17] was included in the modeling. In this model, the equation for the change of radiant intensity, ∂I in an elementary solid along directions ∂x_i can be written as follows:

$$\frac{\partial I}{\partial x_i} = -(\alpha + \sigma_s) I(r,s) + \alpha n^2 \frac{\sigma T^4}{\pi} + \frac{\sigma_s}{4\pi} \int_0^{4\pi} I(r,s)\Phi(s.s')d\Omega' \tag{4}$$

where the right-hand side terms represent local absorption, local emission and scattering transport mechanisms for radiation intensity, respectively. Local absorption and scattering by fluid, wall and PCB are solved using these radiative transport equation couples with the energy equation. Radiation intensity, $I(r, s)$ is directionally and spatially dependent and is determined by a parameter absorption coefficient (α) and scattering coefficient sigma (σ_s). The intensity will decrease due to absorption and out-scattering and increase due to the surface emission of infrared lamp heater and in-scattering. T in the equation represents gas local absolute temperature and σ is the Stefan–Boltzmann constant, which is 5.672×10^{-8} W/m^2 K^4. The equation is written in control volumes and is solved with finite volume method sequentially after solving flow and energy equations.

The gas flow in oven space has dominant flow direction towards fan cage zones and becomes turbulent due to gas flow circulation hitting walls and assembly. From the turbulent CFD methods, the RNG k–ε model with the swirl dominated flow is selected for the model and consist of following two transport equations:

$$\frac{\partial}{\partial t}(\rho k) + \frac{\partial}{\partial x_i}(\rho k u_i) = \frac{\partial}{\partial x_j}\left(a_k \mu_{eff} \frac{\partial k}{\partial x_j}\right) + G_k \tag{5}$$

$$\frac{\partial}{\partial t}(\rho \varepsilon) + \frac{\partial}{\partial x_i}(\rho \varepsilon u_i) = \frac{\partial}{\partial x_j}\left(a_\varepsilon \mu_{eff} \frac{\partial \varepsilon}{\partial x_j}\right) + C_{1\varepsilon}\frac{\varepsilon}{k}(G_k + C_{3\varepsilon}G_b) - C_{2\varepsilon\rho}\frac{\varepsilon^2}{k} - R_\varepsilon \tag{6}$$

In Eq. (5), the terms and G_k represent the turbulence energy production by means of the velocity gradient. The negative term represents the energy dissipation. The RNG based k–ε turbulence model is derived from the Navier–Stokes equation with additional terms of the swirl factor. The swirling flow is accounted by modifying the turbulent viscosity, and it takes the following functional form:

$$\mu = \mu_0 f\left(\alpha_s, \Omega, \frac{k}{\varepsilon}\right) \tag{7}$$

where μ_o is the value of turbulent viscosity calculated without swirl modification. The terms $C_{1\varepsilon}$,$C_{2\varepsilon}$,$C_{3\varepsilon}$ and α_s are the model parameters [18], with the following given values $C_{1\varepsilon} = 1.42$, $C_{2\varepsilon} = 1.68$, Swirl factor, $\alpha_s = 0.07$ and $C_{3\varepsilon} = \tanh|u_2/u_3|$ where u_2 is the component of the flow velocity parallel to the gravitational vector and u_3 is the component of the flow perpendicular to the gravitational vector.

3. Experimental setup and simulation modeling

3.1. Desktop reflow oven

An infrared heating reflow oven with circulating fan was considered for the thermal characteristic investigation. Lau et al. [15] had utilized this reflow oven to investigate the optimization of BGA packaging. However, in-depth study of oven thermal characteristics was not reported in their studies. The investigated reflow oven contains a single temperature zone with multiple temperature segment control (infrared heater). Based on the oven's design, there are maximum sixteen temperature control segments that can be set and stored accordingly. The main parts of the oven consist of six cylindrical shaped infrared tubes, which heat the air. Besides, two circulating fans are used to distribute the hot air inside the oven chamber, and the outlet holes are to release the air out of the oven. Fig. 1 illustrates the experimental setup and schematic diagram of the desktop reflow oven.

The temperature profile is automatically controlled using microcomputer according to the setting temperature. Infrared

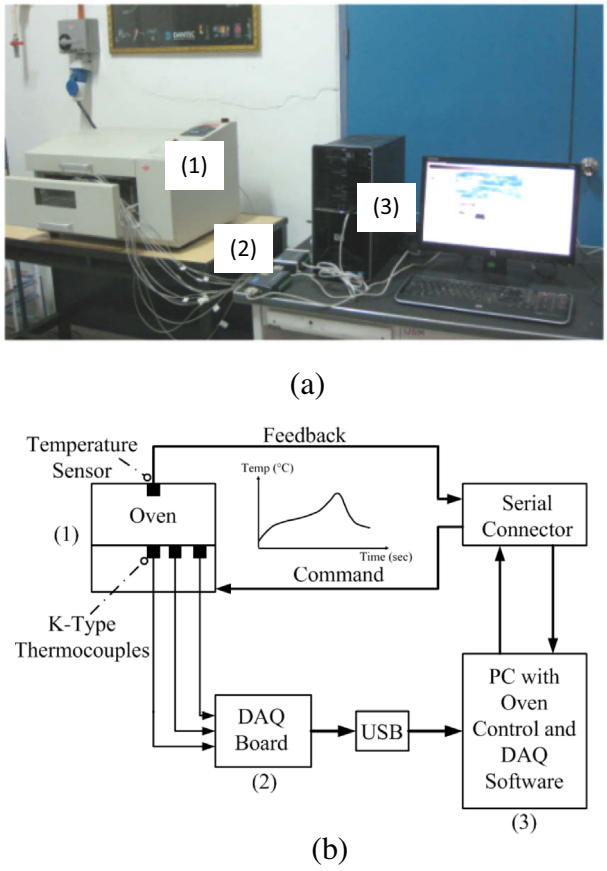

Fig. 1. (a) Experimental setup and (b) schematic diagram of the reflow oven.

heats from the tube are varied according to the setting profile. For the cooling purpose, the infrared heat was reduced significantly, and speed of the fan is increased to force the hot air out of the oven chamber. Fig. 2 shows the geometrical model and the actual view of the circulating fan. The fans are made of stainless steel plate with thickness of 1.5 mm and the total diameter of 115 mm. The blades of the fan consist of ten blades. Each blade has a shape of 90-degree angles with one side facing to the front of the oven, and the other side was perpendicular to it. The workbench area is 350 mm × 250 mm according to the manufacturer. Due to the geometrical symmetry of the oven, only half of the model was considered in detail during numerical simulation studies. During the reflow soldering process, the PCB is static on the plane at the height of 46 mm. The distance between the center of IR tube and bottom of the PCB is 116 mm. The temperature distribution due to convection and radiation is considered during the experiments and the simulations.

Fig. 3 illustrates the reflow soldering profile based on JEDEC JSTD-020D standard [19]. The reflow profile consists of four zones, which are preheating, soaking, reflow and cooling. The recommended duration of the soaking stage is within 60–120 s, and reflow-soldering duration is between 60 and 150 s. The peak temperature setting for the SAC solder material is ranged from 230 to 240 °C. Based on the standard, the setting of the current reflow profile was divided into thirteen sections as shown in Fig. 3. At the reflow section, the temperature ramp up rate and ramp down rate used was less than 2.5 and 3 °C/s, respectively. The detailed temperature and duration setting of each section is summarized in Table 1. In this study, 70 s of preheating time and 90 s of soaking duration and 70 s for the reflow soldering stage were considered.

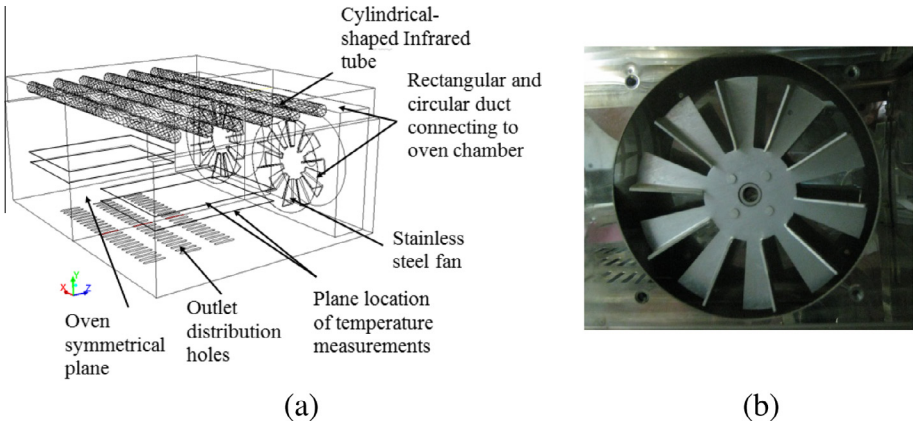

Fig. 2. (a) Geometrical model of desktop reflow oven and (b) actual circulating fan.

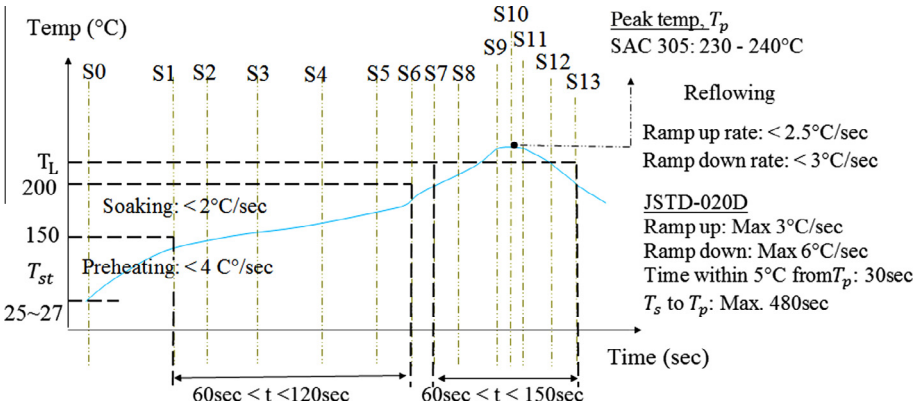

Fig. 3. Setting of the reflow profile for the desktop reflow oven in accordance with JEDEC JSTD-020D standard.

Table 1
Setting temperature of the reflow oven.

Parameter	Preheating		Soaking					Reflowing						
	Start	S1	S2	S3	S4	S5	S6	S7	S8	S9	S10	S11	S12	S13
Temperature (°C)	27	150	160	170	180	190	200	220	225	227	230	228	225	220
Duration (s)	0	70	20	20	20	20	10	10	10	10	10	10	10	10
|Max. gradient (°C/s)|		1.7	0.5	0.5	0.5	0.5	1.0	2.0	0.5	0.2	0.3	0.2	0.3	0.5

3.2. Temperature distribution assessment

The uniformity of oven chamber temperature was determined from the recorded temperatures, and it was calculated as the temperature difference between the setting temperatures. The experiment was designed because no literature reported on the experimental thermal investigation of the desktop reflow soldering process. The initial temperature inside the chamber was controlled and determined to be in a range of 25–27 °C. Experiments were carried out for the validation of the numerical model. The numerical model can be considered credible to the extent to which it was validated against reliable measurement data.

To record the temperature distribution of the oven chamber, a total of 60 thermocouples' locations was measured at selected plane. The thermocouples were placed at two different heights within the oven chamber. These thermocouples were positioned on a plane 61 mm (lower layer or oven rack) and 76 mm (upper layer, 15 mm above oven rack) from the bottom wall of the chamber. The thermocouple array for each plane was divided into three columns. During the experiments, twelve thermocouples, which located in each column as illustrated in Fig. 4(a), measure the temperature of each running. The experiment was repeated, and the average values were computed for each plane. At certain positions, overlapping thermocouples were used to calculate the average values and the experiments were repeated to determine the repeatability of reflow setting. The thermocouple arrays were attached to the stainless steel frames and hold in finite position using Kapton tape as shown clearly in Fig. 4(b). Experimental uncertainty analysis was conducted to estimate the percentage error of measurement. Measurements were repeated using one thermocouple at the selected position. The measurement at the position is selected as a reference value. The procedure is repeated with the increasing number of thermocouples surrounded the reference position until, a total number of thermocouples have been reached. Finally, the temperature measurements of the reference position are compared, and maximum temperature deviation is less than 1%. Moreover, the smaller size of thermocouple was used for the comparison and the difference in measurement is less than 3%. Finally,

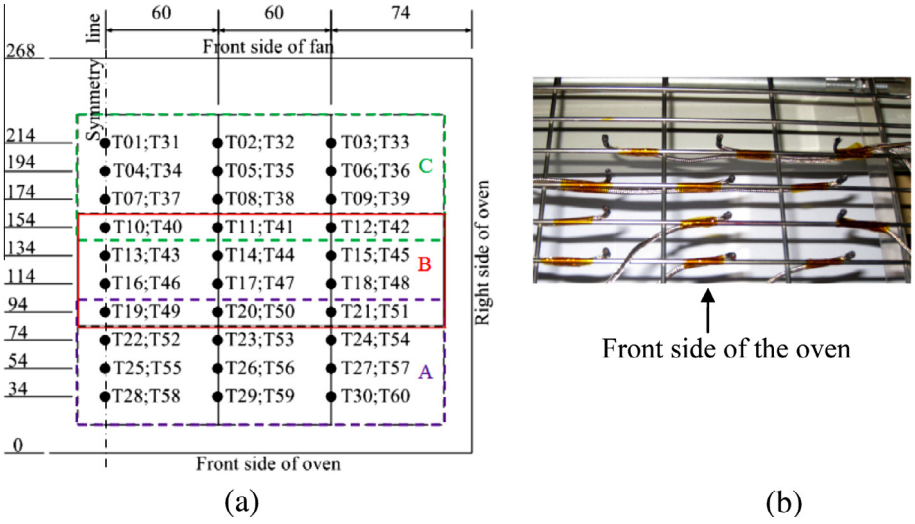

Fig. 4. (a) The distribution of thermocouples on the lower layer (T01–T30) and upper layer (T31–T60) for the temperature validation in the oven chamber. The dimensions are given in millimeters. (b) Thermocouple setting for T10–T21 (B column).

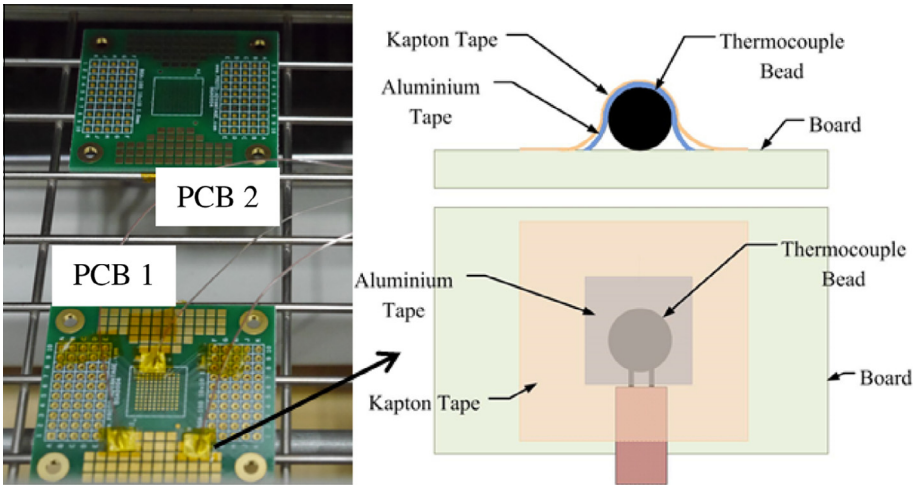

Fig. 5. Locations of the FR-4 PCB during the measurement experiment.

the thermocouple diameter size of 0.5 mm was selected for measurement of bulk air temperature from the oven to stabilize unwanted fluctuations from the smaller size of thermocouple.

3.3. Temperature measurement on the PCB

High-temperature FR-4 printed circuit board (PCB) with dimensions of 48 mm × 53 mm × 1.6 mm was used as a test board in the temperature measurement experiment. Two identical test boards were arranged at the front (46 mm from the front side of the oven) and back (134 mm from the front side of the oven) locations as depicted in Fig. 5. Each test board was instrumented with three type-K thermocouples, which attached using aluminum tape in combination with Kapton tape to provide a secure connection with good thermal conductivity between board and thermocouple bead. Aluminum tape was cut to the size of approximately 5 mm × 5 mm and was used to secure the thermocouple to the PCB. The aluminum taped was then overlaid with 8 mm × 8 mm of Kapton tape to prevent lifting (Fig. 5). The thermocouples will measure the temperature of PCB surface by running the setting thermal profiles. For each PCB position, average values were computed, and the peak temperature data of PCB during reflow were extracted. The temperature assessment of the measurement was used to validate the numerical model.

3.4. FLUENT modeling

The three-dimensional (3D) oven model was constructed based on the actual dimension of the desktop reflow oven as illustrated in Fig. 2(a) (in Section 3.1). The model was solved by using the finite volume based solver [20]. The geometrical model, which is described in Section 2, was discretized using a high-quality mesh. Due to large differences in size and attribute between particular parts of the heating oven (e.g., fan geometry, heater, outlet distribution holes and oven height), the size function of the grid generation was required. The size function was used in the vicinity of all outlet holes, cylindrical shaped heaters, and fan. The size of the element in outlet holes and around heaters vicinity is 1 mm only with growth size factor of 1.3. General size element set in the oven chamber is 6 mm. In fan chamber, a general element size of 1 mm is set to all elements in a radius of 63.5 mm from the center of fan, whereas 6 mm general element size is set for the remaining volume. Almost all elements of the grid were tetrahedrons. Quality check of all elements shows that there are less than

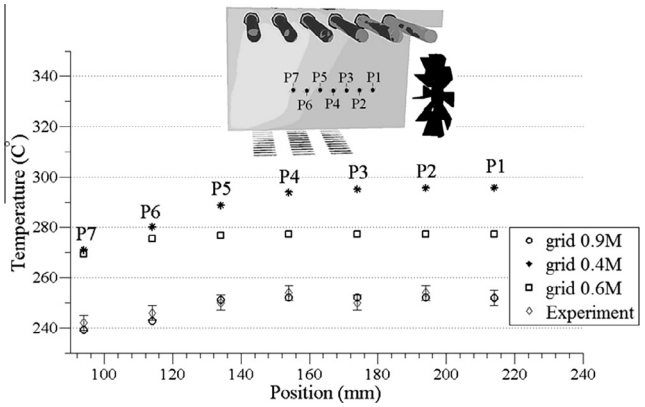

Fig. 6. Temperature distribution at points (P1–P7) for various mesh sizes.

0.01% of total elements have aspect ratio more than 3. The preliminary computations were performed for three meshes with a gradually increasing number of elements to check the mesh independence. The meshes with 0.4 million, 0.6 million and 0.9 million were used for basic configuration of the computational oven model. Fig. 6 shows the temperature (peak temperature during reflow stage) plotting of finite points (P1–P7) for three different mesh sizes as compared with the experimental results.

As a comparison with experimental results, it is observed that meshes with 0.4 million elements (grid 0.4 M) and 0.6 million elements (grid 0.6 M) have large nominal deviation. As a result of these tests, the grid with the 0.93 million number of elements was selected for further study. In order to complete the computational model formulation, the flow, and thermal boundary conditions must be specified on the model boundaries. The following boundaries and initial conditions at model boundaries can be distinguished:

(a) At the fan: The flow features associated with rotating parts of the fans are modeled using multiple reference frames in ANSYS Fluent. The multiple reference frames are defined on the blade in the fan cage domain. Rotation with an angular velocity of 150 rad/s is defined on the blades based on average measurement value using HT50 tachometers.
(b) At outlet holes: The outlet holes located on the bottom of the wall (Fig. 2(a)). For this boundary, the pressure outlet boundary condition was defined at the atmospheric pressure (P = 1 atm).
(c) On infrared lamp heaters: Polynomial heat flux profiles were prescribed uniformly on the outer surface of each heater based on power output recorded during experiments. Based on the values from experiments, heat flux of infrared lamp heaters is calculated. Considering the lamps as a source of heat to the system, flux is calculated based on the lamp power. For example, the average power of each lamp is 100 W. The surface area of the lamp cover is approximately 0.017 m^2, which will give a flux of 5.8 kW/m^2 nominal average values. Advanced user-defined functions (UDFs) of polynomial profile based on the experimental setting were developed using C program and incorporate into the FLUENT simulation.
(d) On the external wall and PCB surface: The external wall of the device surrounded by PCB in the oven is defined by an emissivity value of 0.1 [21] on the wall and 0.9 [22] for the PCB.
(e) On the symmetrical plane: Due to the symmetrical condition of the oven, only half plane symmetry is considered during the simulation to save the computational time. The temperature gradient and velocity of air across the plane are considered minimal and ignored. Specifically, on that plane; $\frac{\partial u_1}{\partial x} = \frac{\partial u_2}{\partial x} = \frac{\partial u_3}{\partial x} = \frac{\partial T}{\partial x} = 0$ are defined.

4. Results and discussion

4.1. Temperature distribution of reflow oven

The temperature distribution of the reflow oven was evaluated experimentally, and the results are presented in three-dimensional plots as shown in Fig. 7. Temperature at preheating, soaking and reflow stage was considered at 150, 200 and 230 °C, respectively. The temperature at two different heights (i.e., lower layer and upper layer) was measured by the thermocouple array. In Fig. 7, the positive value of the temperature difference indicated that the measured temperature is higher than the profile temperature setting and vice versa for the negative value. The temperature difference of the oven chamber exhibits non-homogenous temperature distribution along the front distance. The results reveal the upper layer has a higher temperature difference than the lower layer, which attribute to the closer distance of the upper layer with the infrared heaters. Besides, speed of circulating fan may also contribute to the inhomogeneous temperature distribution in the desktop reflow oven. As expected, the temperature difference increases when the setting temperature increased at various stages.

Moreover, two phenomena were observed from the experimental results, which are (i) extremely overshooting temperature in the region that closer to the fan and (ii) lower temperature around the front workbench region. These scenarios revealed the possible over and insufficient heating on the PCB and component when using the reflow oven. The extremely high temperature will cause the unintended effects on the solder joints, such as an increase the thickness of IMC, causing burn mark on the PCB and component. However, low temperature may lead to inadequate heating of the solder material; hence induce the unbaked solder joint. Therefore, an alternative way to overcome this problem is to offset the profile setting and select the appropriate position based on the experimental results. These experimental results are useful for the designer to improve the oven design and as a reference for the researcher when using the desktop reflow oven.

4.2. Temperature contour

Temperature field of the oven chamber is only able to capture using the thermocouple at a certain position. The temperature contour is difficult to visualize in the experiment. Thus, the simulation analysis was carried out to study the temperature contour of the oven chamber. Fig. 8(a) shows the temperature contour of the oven chamber and seven points (P1–P7) were selected for the comparison with experimental results. The temperature contour is displayed in the middle cross-section of the oven chamber during the reflow stage. The simulation results revealed that higher temperatures are detected in back region (closer to the fan) rather than front region of the oven. This situation verified the phenomena that have been observed in the experiments (Section 3.1). Besides, the experimental results substantiated the predicted temperature of the current simulation, as illustrated in Fig. 8(b). The discrepancy between both results was less than 5%.

Inhomogeneous of chamber temperature was further investigated numerically. During the reflow process, the higher temperatures are shifted to the back region (closer to the fan) due to air circulation from the middle side towards the fan cage. The air close to the bottom wall of the chamber re-circulates at the back region. A partial hot air from the front region exits the chamber

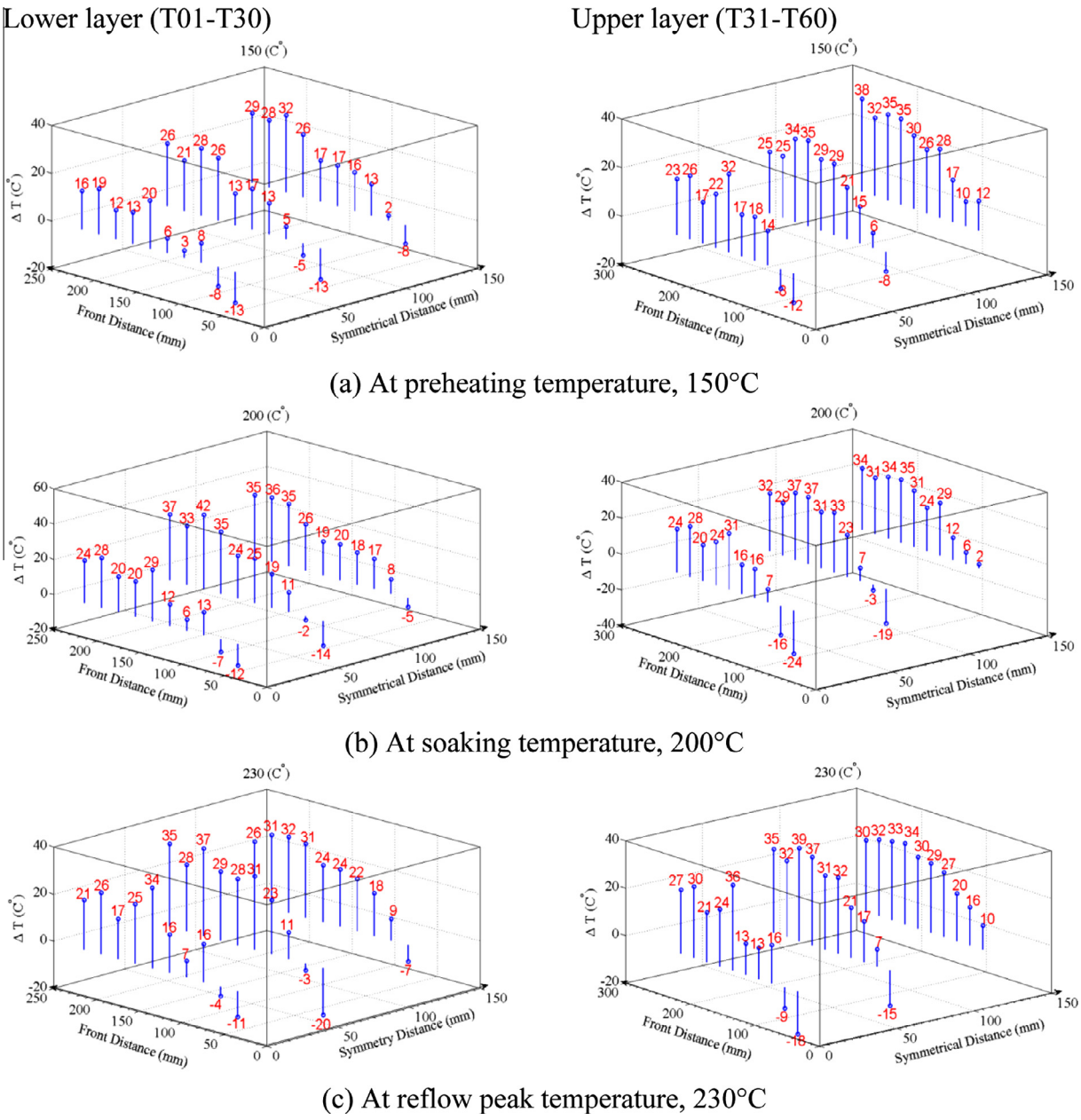

Fig. 7. Temperature difference at lower layer (T01–T30) and upper layer (T31–T60).

through the outlets, which are positioned in the range of 35–165 mm from front oven. From the results, the temperature variations in the oven chamber were ascribed to the outlet design. Outlet around the front region is causing the temperature drop drastically and lead to non-homogeneity of temperature distribution in the entire oven chamber. This scenario is clearly explained by the flow mechanism and velocity vector as illustrated in Fig. 9.

In addition, the unique design of fan blades forces the air to move parallel to the shaft. The airflow from the oven chamber is circulated and moves horizontally into the fan cage, revolves around the blade propeller and flow vertically upwards out of the fan cage. The airflow at heater space is heated up to approximately to heater temperature. Then the airflow moved downwards and directed back to the fan chamber. The heat transferred from the top to bottom, heating the air first and stratifying from the ceiling downward. The plane view in Fig. 9 shows that the continuous flow forms circular motion directed to the fan cage. The blade rotation creates a suction force into the fan cage throughout the reflow process. This flow mechanism enables the air circulation and heat distribution from the IR heater to the PCB during the desktop reflow soldering process.

4.3. Effect of fan speed and PCB position

The study was extended to investigate the fan speed using the simulation modeling technique. The homogeneity of the temperature distribution may influence by several factors such as temperature profile setting, fan speed, and oven design. Temperature overshooting in the oven chamber may depend on the flow circulation as discussed in Section 3.2. Therefore, the circulating fan speed was considered at different Reynolds numbers. The Reynolds number for the fan impeller oven is defined as

$$\mathrm{Re} = \frac{\rho D^2 n}{\mu} \tag{8}$$

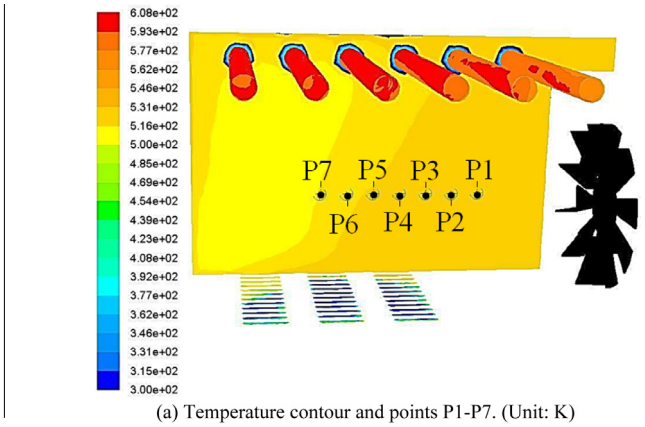

(a) Temperature contour and points P1-P7. (Unit: K)

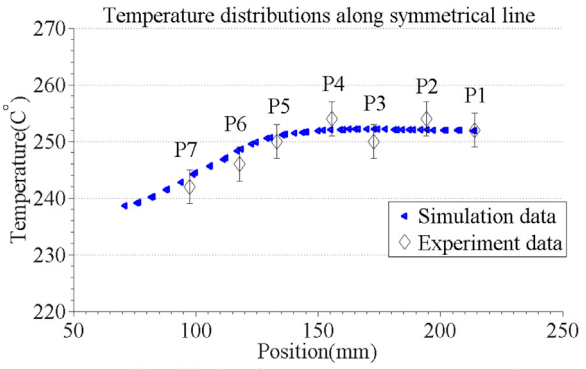

(b) Validation of temperature measurement at points P1-P7.

Fig. 8. Comparison of temperature measurement in simulation and experimental results.

where D is the fan diameter, n is RPM of the fan, ρ is density of the fluid and μ is viscosity of the fluid.

PCB surface temperature during reflow at peak temperature as a function of Reynolds number was computed. The correlation of Reynolds number and average peak surface temperature of the PCB according to the defined positions were analyzed and plotted in Fig. 10. The results discovered the effects of selected positions on PCB surface temperature. At low Reynolds number, the PCB1 and PCB2 experienced high surface temperatures, 260 and 290 °C, respectively. The average surface temperature of PCB1 decreases proportionally at Reynolds numbers 0.35×10^5 until 1.35×10^5. After Reynolds number 1.35×10^5, the PCB surface temperature exhibits nearly constant at 235 °C. Once the Reynolds number increased, the surface temperature (PCB2) drops gradually until 250 °C at 2.75×10^5 of Reynolds number. These two correlations demonstrate the significance of fan speed control in order to achieve better temperature uniformity and desired reflow temperature (230 °C $\leqslant T <$ 240 °C) when using the desktop reflow oven with circulating fan. Besides, the PCB located in the front region is favorable to the temperature homogeneity and targeted reflow temperature. The simulation results for both PCBs at 1.425×10^5 of Reynolds number were validated by experimental measurement value.

Fig. 11 shows the temperature contour of the oven chamber in a plane view. The PCB2 endured to a higher temperature than PCB1. This phenomenon can be explained based on the airflow circulation as mentioned in Section 3.2. The airflow in the front region exits oven chamber through the outlets caused lower temperature than back region. In addition, two PCBs at two positions were used to verify the observation in the simulation by using the similar reflow profile setting at 1.425×10^5 of Reynolds number. In the reflow experiment, PCB1 experienced lower temperature than PCB2. Thus, no burn mark was observed on the PCB1. The simulation result also discovered that the temperature distributes non-uniformly on PCB2, nearly half of PCB2 surface subjected to the upper limit 280 °C, which is 11 °C higher compared to the other lower surface area. PCB2 endured to the high temperature that exceeds the setting temperature during the reflow process. Thus, PCB2 was overheated, and brown burn mark was markedly observed on the surface of the PCB, as shown in Fig. 12(a).

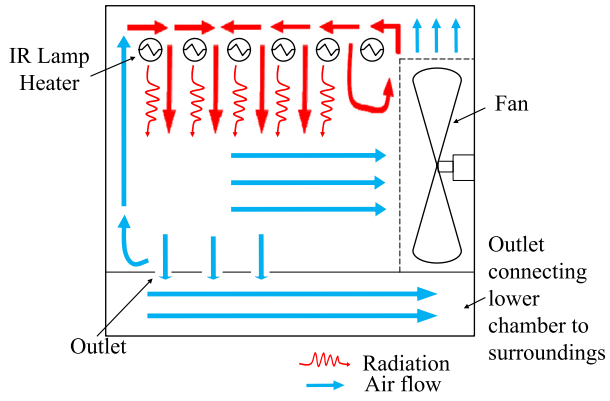

(a) Flow mechanism on a plane

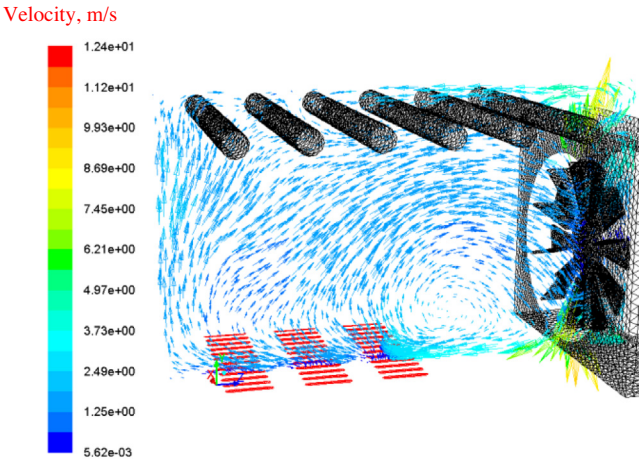

(b) Velocity vector at the centre plane

Fig. 9. Circulating flow in the oven during the reflow soldering process.

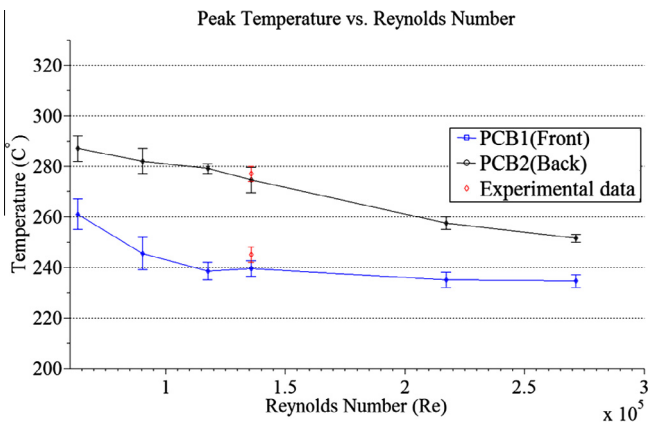

Fig. 10. Temperature of two PCBs at different Reynolds number in reflow stage.

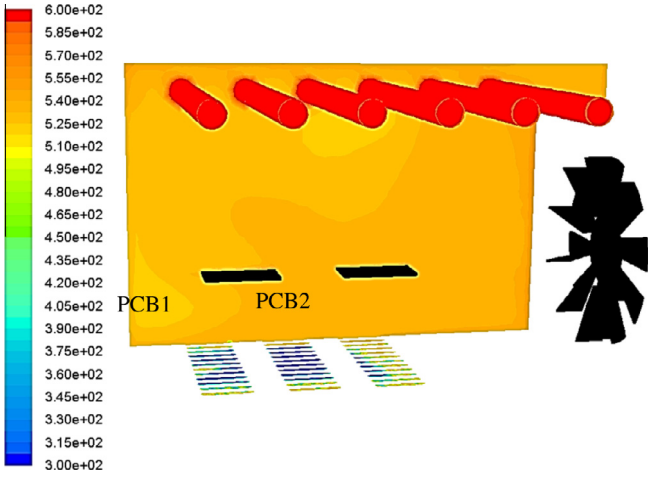

Fig. 11. Temperature contour of the oven chamber, PCB1 and PCB2 at reflow stage.

Temperature contour (Fig. 12(b)) shows a higher temperature in the upper PCB region (area between corner 3 and 4) where the defect takes place. The peak temperature value is clearly far beyond the setting temperature (230 °C). The heat transfer coefficient of the PCB2 is presented 2D contour plot as shown in Fig. 12(c). The PCB2 overheated region (between 3 and 4) has the highest heat transfer coefficient value (above 280 W/m^2 K). This indicated that PCB2 experienced a large amount of heat transferred from the environment to the PCB, which due to the inhomogeneous temperature distribution of the reflow oven. This scenario is unfavorable during the reflow soldering process. In addition, extremely high reflow temperature degrades the solder joint and lead to other component failures during the reflow soldering process. Therefore, the researcher must concern these aspects when using the desktop reflow oven with circulating fan.

5. Conclusion

The investigations of the thermal process for the desktop reflow oven were carried out in the experiment and numerical simulation. The temperature distribution of the oven chamber was evaluated using a set of thermocouple array during the reflow process. The reflow profile was set in accordance with the JEDEC JSTD -020D standard. The experimental results revealed the temperature distribution in the oven chamber was inhomogeneous, which

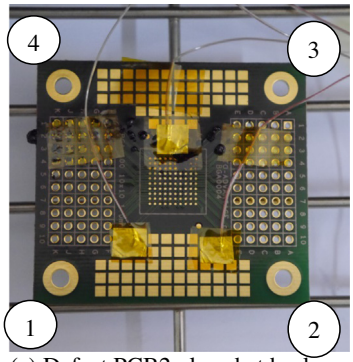

(a) Defect PCB2 placed at back region of oven.

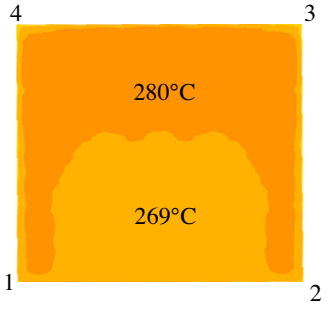

(b) PCB2 Temperature Contour.

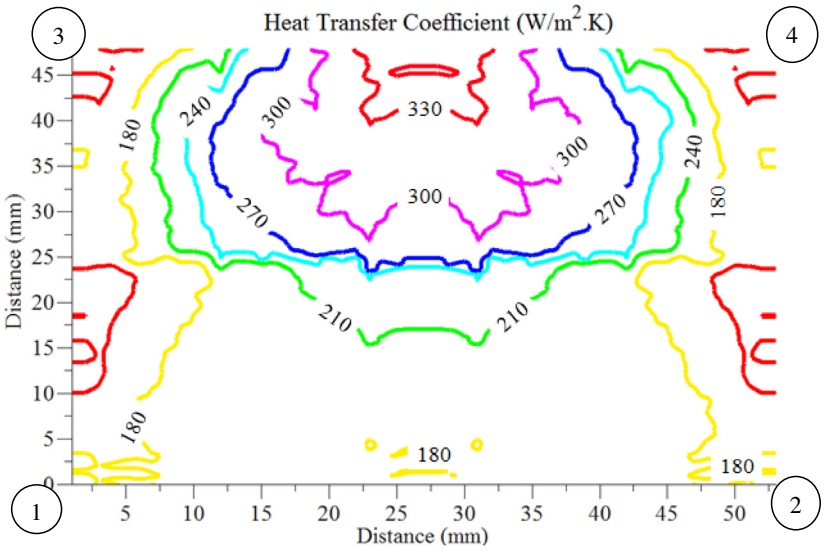

(c) PCB2 heat transfer coefficient contour.

Fig. 12. The overheated PCB due to non-homogeneous temperature distribution.

temperature is higher in the back region and lower in the front region. This situation was attributed to air circulation in the oven chamber. The presence of the outlets in the front region allows the hot air exits from the chamber, which causes the lower temperature in that region. Besides, the air circulation mechanism was clearly demonstrated in the numerical simulation. The better temperature uniformity and targeted PCB surface temperature ($230\ ^\circ C \leqslant T < 240\ ^\circ C$) could be achieved at high Reynolds number (1.35×10^5 to 2.75×10^5) when the PCB located in the front region. Moreover, the defect of overheated PCB in back region was demonstrated in the experiment, whereas the PCB experiences high temperature than the setting temperature during the reflow process. Both experiment and simulation showed a satisfactory agreement for the temperature of the oven chamber. Thus, these results are useful for the oven designer to improve the thermal performance of the desktop reflow oven and as a reference for the researcher when using the reflow oven.

Conflict of interest

None declared.

Acknowledgments

The author would like to thank the Ministry of Higher Education Malaysia through Universiti Teknikal Malaysia Melaka for the Ph.D. scholarship program.

References

[1] R.C. Dorf, The Electrical Engineering Handbook, third ed., Taylor & Francis Group, Boca Raton, 2006.
[2] J. Pan, T.C. Chou, J. Bath, D. Willie, B.J. Toleno, Effects of reflow profile and thermal conditioning on intermetallic compound thickness for SnAgCu soldered joints, Soldering Surface Mount Technol 21 (4) (2009) 32–37.
[3] D. Bao, How to minimize defects by adjusting the reflow profile, Metallic Resources, Inc., 2014, pp. 1–4. Retrieved from http://metallicresources.com/ [Accessed 11 July 2014].
[4] L. Gao, S. Xue, L. Zhang, Z. Sheng, F. Ji, W. Dai, S.L. Yu, G. Zeng, Effect of alloying elements on properties and microstructures SnAgCu solders, Microelectron. Eng. 87 (11) (2010) 2025–2034.
[5] C.M.T. Law, C.M.L. Wu, D.Q. Yu, L. Wang, J.K.L. Lai, Microstructure, solderability, and growth of intermetallic compounds of Sn–Ag–Cu-RE lead-free solder alloys, J. Electron. Mater. 35 (1) (2006) 89–93.
[6] B. Illés, Measuring heat transfer coefficient in convection reflow ovens, Measurement 43 (2010) 1134–1141.
[7] B. Illés, G. Harsányi, Investigating direction characteristics of the heat transfer coefficient in forced convection reflow oven, Exp. Therm. Fluid Sci. 33 (4) (2009) 642–650.
[8] B. Illés, G. Harsányi, Heating characteristics of convection reflow ovens, Appl. Therm. Eng. 29 (11–12) (2009) 2166–2171.
[9] B. Illés, G. Kristóf, L. Jaka, Thermal and gas flow characterization of a fluxless Si solder bonding oven, Exp. Therm. Fluid Sci. 35 (1) (2011) 29–36.
[10] B. Illés, Distribution of the heat transfer coefficient in convection reflow oven, Appl. Therm. Eng. 30 (2010) 1523–1530.
[11] B. Illés, A. Géczy, Multi-physics modelling of a vapour phase soldering (VPS) system, Appl. Therm. Eng. 48 (2012) 54–62.
[12] B. Illés, A. Géczy, Investigating the dynamic changes of the vapour concentration in a vapour phase soldering oven by simplified condensation modeling, Appl. Therm. Eng. 59 (2013) 94–100.
[13] A. Géczy, B. Illés, Z. Illyefalvi-Vitéz, Modeling method of heat transfer during vapour phase soldering based on filmwise condensation theory, Int. J. Heat Mass Transfer 67 (2013) 1145–1150.
[14] B. Illés, A. Géczy, Numerical simulation of condensate layer formation during vapour phase soldering, Appl. Therm. Eng. 70 (2014) 421–429.
[15] C.S. Lau, M.Z. Abdullah, C.Y. Khor, Optimization of the reflow soldering process with multiple quality characteristics in ball grid array packaging by using the grey-based Taguchi method, Microelectron. Int. 30 (3) (2013) 151–168.
[16] J. Smolka, Z. Bulinski, A.J. Nowak, The experimental validation of a CFD model for a heating oven with natural air circulation, Appl. Therm. Eng. 54 (2013) 387–398.
[17] ANSYS Inc, ANSYS FLUENT User's Guide Release 14.0, 2011.
[18] S.A. Orszag, V. Yakhot, W.S. Flannery, F. Boysan, D. Choudhury, J. Maruzewski, B. Patel, Renormalization Group modeling and turbulence simulations, in: Conference on Near-Wall Turbulent Flows, Arizona, 1993, pp. 1031–1046.
[19] IPC/JEDEC JSTD-020D.1, March 2008, Joint IPC/JEDEC standard for moisture/reflow sensitivity classification for non hermetic solid state surface mount device, Retrieved from http://www.jedec.ord/standards-documents/results/j-std-020 [Accessed 11 August 2014].
[20] B. Illés, I. Bakó, Numerical study of the gas flow velocity space in convection reflow oven, Int. J. Heat Mass Transfer 70 (2014) 185–191.
[21] F. Cverna, ASM Ready Reference: Thermal Properties of Metals, first ed., ASM International, Ohio, 2002. pp. 526–527.
[22] P. Svasta, D.S. Zanescu, R. Ionescu, Components' emissivity in reflow soldering process, Electron. Compon. Technol. Conf. (2004) 1921–1924.